Estuarine, Coastal and Shelf Science 140 (2014) 52–65

Contents lists available at ScienceDirect

Estuarine, Coastal and Shelf Science

journal homepage: www.elsevier.com/locate/ecss

# Mercury dynamics in a coastal aquifer: Maunalua Bay, O'ahu, Hawai'i

Priya M. Ganguli [a,*], Peter W. Swarzenski [b], Henrieta Dulaiova [c], Craig R. Glenn [c], A. Russell Flegal [a]

[a] University of California, Santa Cruz, WIGS Lab, Earth Sciences Department, Santa Cruz, CA 95064, USA
[b] US Geological Survey, Pacific Coastal & Marine Science Center, 400 Natural Bridges Drive, Santa Cruz, CA 95060, USA
[c] University of Hawai'i, Department of Geology and Geophysics, Honolulu, HI 96822 USA

ARTICLE INFO

*Article history:*
Received 23 September 2013
Accepted 29 January 2014
Available online 5 February 2014

*Keywords:*
mercury
estuarine chemistry
coastal waters
groundwater
mixing processes
groundwater–surface water interaction

ABSTRACT

We evaluated the influence of groundwater–seawater interaction on mercury dynamics in Maunalua Bay, a coral reef ecosystem located on the south shore of O'ahu, Hawai'i, by combining geochemical data with submarine groundwater discharge (SGD) rates. During a rising tide, unfiltered total mercury (U-HgT) concentrations in seawater increased from ~6 to 20 pM at Black Point (west Bay) and from ~2.5 to 8 pM at Niu (central Bay). We attribute this change to an increase in suspended particulate matter at high tide. Approximately 90% of mercury in groundwater at Niu was in the filtered (<0.45 μm) fraction, with a concentration of ~4 pM. Groundwater discharge during a period of amplified SGD at Niu appeared to contribute to an increase in total mercury concentrations in filtered seawater (F-HgT; 1.2 to 2.4 pM) and in unfiltered seawater (U-HgT; 2.5 to 3.2 pM). The larger magnitude of change in F-HgT relative to U-HgT suggests mercury complexation and/or solubility dynamics in seawater were altered by the addition of groundwater. We used site specific $^{222}$Rn derived SGD flux estimates and groundwater F-HgT concentrations to calculate mercury loadings at Black Point (~3 nmol m$^{-2}$ d$^{-1}$) and at Niu (~1 nmol m$^{-2}$ d$^{-1}$). We calculated a weighted average Maunalua Bay groundwater mercury flux of 0.68 ± 0.67 mol yr$^{-1}$ by combining the proportional flux of F-HgT from three distinct SGD zones, and place these results into a broader context by comparing and contrasting flux estimates from locations around the world. Results from existing SGD studies should be evaluated to develop future sampling strategies that address more targeted questions about mercury biogeochemical cycling at the groundwater–seawater interface.


## 1. Introduction

Local sources of mercury on the Hawaiian Islands in the North Pacific Ocean include volcanic emissions as well as the historic use of antifouling paint, agricultural fungicides, ammunition, and fireworks (Siegel and Siegel, 1984; Raine et al., 1995). Mercury is also introduced through atmospheric deposition associated with global fossil fuel combustion (Pacyna et al., 2010). Although the majority of this mercury is inorganic (Hg(II)), some anaerobic bacteria can convert Hg(II) into monomethylmercury ($CH_3Hg^+$, referred to herein as MMHg), a neurotoxin that readily biomagnifies in the food web (Benoit et al., 2003). Mercury bioaccumulation and biomagnification in aquatic ecosystems is typically more efficient than in terrestrial systems because of the structure and complexity of aquatic food webs and the physiology of many aquatic organisms (USEPA, 1997; Davis et al., 2003). Therefore, biologically productive coastlines, such as Hawaiian coral reef ecosystems, may be particularly susceptible to mercury inputs (see Section 4.5).

A number of studies have quantified the flux of submarine groundwater discharge (SGD) to the coastal waters of Hawai'i and identified SGD as an important source of contaminants (e.g., Hoover and Mackenzie, 2009; Peterson et al., 2009; Knee et al., 2010; Dimova et al., 2012; Swarzenski et al., 2013). However, little is known about nearshore mercury dynamics in this region. The flux of mercury via SGD has been measured at just a handful of locations around the world, including sites in France (Laurier et al., 2007), the United States (east and west coasts) (Bone et al., 2007; Black et al., 2009; Ganguli et al., 2012), Korea (Lee et al., 2011; Rahman et al., 2013), and the Baltic Sea (Szymczycha et al., 2013). Although atmospheric deposition of Hg(II) and subsequent methylation in the upper waters of the open ocean appears to be the primary source of monomethylmercury (MMHg) in the global marine food web (Mason et al., 2012; Blum et al., 2013), results from

* Corresponding author. Present address: Woods Hole Oceanographic Institution, Mail Stop #51, Marine Chemistry and Geochemistry Department, Woods Hole, MA 02543, USA.
*E-mail addresses:* pganguli@whoi.edu (P.M. Ganguli), pswarzen@usgs.gov (P. W. Swarzenski), hdulaiov@hawaii.edu (H. Dulaiova), glenn@soest.hawaii.edu (C. R. Glenn), flegal@ucsc.edu (A.R. Flegal).

0272-7714/$ – see front matter © 2014 Elsevier Ltd. All rights reserved.
http://dx.doi.org/10.1016/j.ecss.2014.01.012

SGD-mercury studies suggest that in many locations, export from coastal aquifers contributes to local mercury budgets and can affect nearshore mercury biogeochemical cycling (Bone et al., 2007; Laurier et al., 2007; Black et al., 2009; Ganguli et al., 2012; Rahman et al., 2013; Szymczycha et al., 2013).

In this paper, we consider the influence groundwater–seawater interaction has on mercury dynamics in the coastal waters of Maunalua Bay along the south shore of O'ahu (Fig. 1). This coral reef habitat has recently been impacted by widespread urban development (Wolanski et al., 2009; Storlazzi et al., 2010; Presto et al., 2012; Swarzenski et al., 2013). We monitored ~hourly changes in filtered and unfiltered total mercury (HgT) concentrations in nearshore groundwater and seawater, and documented the geochemical response of these water masses to tidal perturbations. Additionally, we present the first estimates of groundwater mercury fluxes to a coral reef ecosystem and consider the potential for

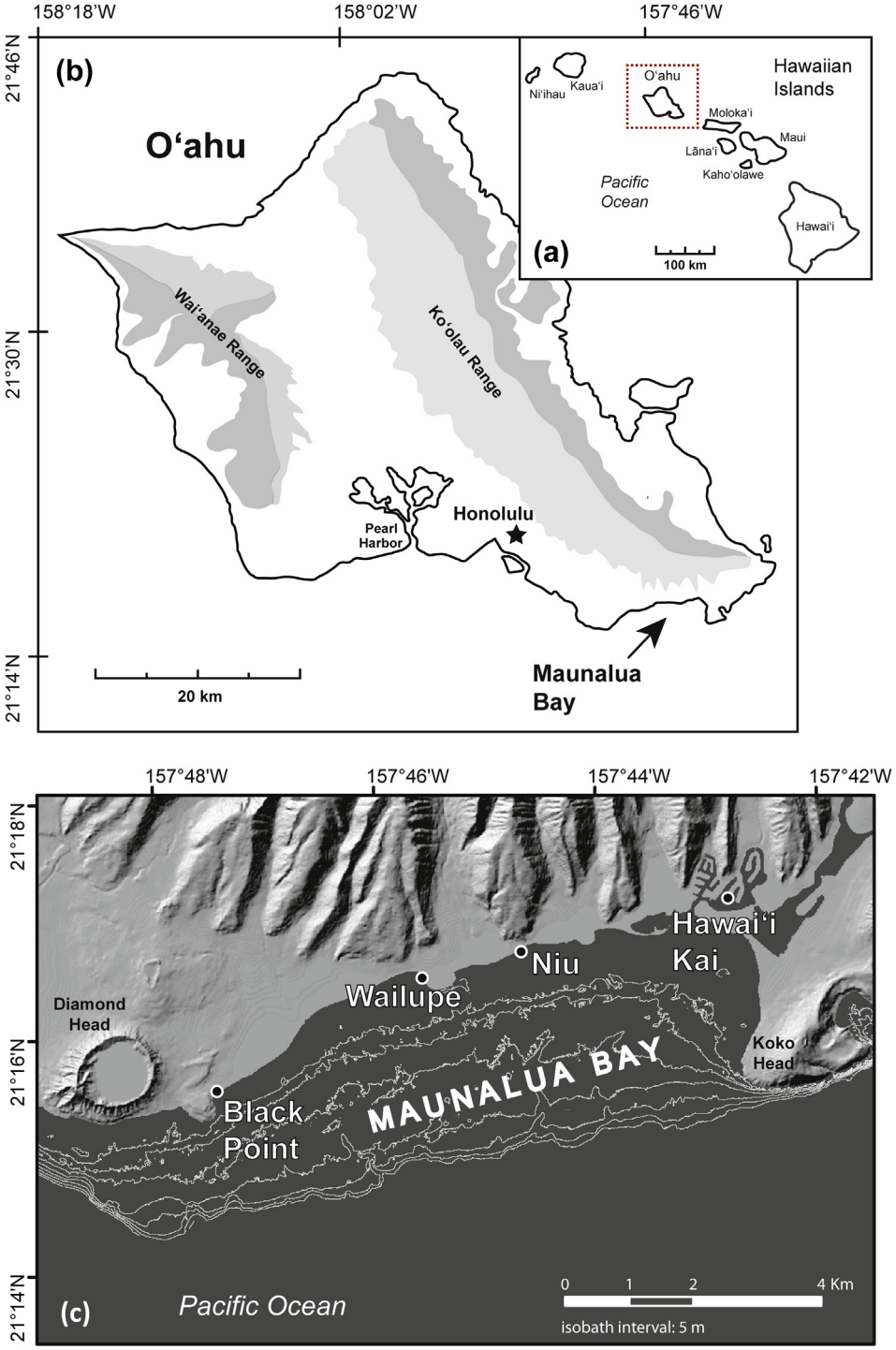


**Fig. 1.** (a) Site location map of the Hawaiian Islands in the North Pacific Ocean. (b) The island of O'ahu showing the Maunalua Bay study area. (c) Detailed map of Maunalua Bay, identifying our sampling locations. The submarine groundwater discharge (SGD) flux estimates were made at Black Point, Niu, and Hawai'i Kai using U/Th isotopic methods and at Wailupe using electrical resistivity. Water samples for geochemical analyses were collected at Black Point and Niu.

MMHg production given the geochemical and hydrological characteristics of Maunalua Bay. Finally, we compare and contrast HgT flux estimates from a range environments and consider how sampling strategies can be employed to evaluate targeted questions about mercury cycling in coastal systems.

## 2. Theory

Tidal changes can play a large role in driving groundwater discharge and seawater recirculation in many coastal environments (Swarzenski and Kindinger, 2003; Moore, 2010). During low tide, the slope of the hydraulic gradient is maximized in the seaward direction (assuming baseflow conditions), resulting in enhanced groundwater discharge rates. If the groundwater flux is high enough to overcome physical and biological drivers (e.g., coastal flushing, uptake by organisms), the geochemical composition of nearshore seawater can shift toward that of the groundwater end member. The timing of peak discharge may precede or lag behind low tide based on aquifer properties and the hydrodynamics of the system. As the tide rises, the slope of the hydraulic gradient decreases and groundwater discharge decreases, enabling seawater to infiltrate coastal sediment and rock. In such a case, the nearshore groundwater geochemical signature will presumably shift towards that of seawater.

To determine the timing and rate of SGD in Maunalua Bay, we employed a combination of radioisotope mass balance calculations (Swarzenski et al., 2013) and electrical resistivity imaging (Dimova et al., 2012). The short-lived (half-life = 3.8 days) radioactive element radon ($^{222}$Rn) occurs naturally in sediment and is therefore present at elevated concentrations in groundwater relative to seawater. The flux of SGD can be estimated by developing a transient box model of radon input and loss terms, based on time-series monitoring of the activity of radon in seawater over multiple tidal cycles (Swarzenski et al., 2013). Measurements of electrical resistivity in nearshore pore water can also be used to characterize the fresh water-salt water interface and the scales and dynamics of SGD. Coastal groundwater typically has lower conductivity than seawater and therefore higher electrical resistivity. Consequently, time lapse images of subsurface resistivity can document changes in the groundwater–seawater mixing prism over time and this information can be used to infer rates of SGD (Dimova et al., 2012).

## 3. Materials and methods

### 3.1. Study area

Maunalua Bay is located along the southern shore of Oʻahu, Hawaiʻi, approximately 10 km east of Honolulu (Fig. 1). Wolanski et al. (2009) describe the recent urbanization that has occurred throughout the coastal plain of Maunalua Bay and along nearby hillsides at the base of the Koʻolau Range. Development of the range's erodible slopes combined with stream channelization and hardening have substantially increased sediment runoff to the Bay. The receiving watershed is also impaired by elevated concentrations of nutrients, metals, fertilizers, and pesticides associated with urban development (e.g., septic systems, landscaping) and agricultural practices (Frans et al., 2012; Swarzenski et al., 2013). The multiplicity of these impacts on Maunalua Bay has resulted in a collapse of its coral reef ecosystem (Wolanski et al., 2009).

Studies to characterize sediment dynamics (Storlazzi et al., 2010) and coral-larval transport (Presto et al., 2012) in Maunalua Bay found that circulation in the Bay is driven by trade-winds and is primarily to the west. Turbidity in the water column appears to be linked to wave action and storm events, as well as tidal fluctuations (Wolanski et al., 2009). However, observed increases in suspended matter are short-lived, possibly due to particle transport off-shore by large south swell events that flush the Bay (Storlazzi et al., 2010). The residence time of water in the western and central portion of Maunalua Bay is less than a day (Wolanski et al., 2009; Presto et al., 2012). On the eastern side, sedimentation and physical modifications have restricted water circulation and intensified the sheltering effect of Koko Head peninsula, which forms a cove in the northeastern region (Fig. 1c). As a result, water in east Maunalua Bay has a residence time of about a week (Wolanski et al., 2009; Presto et al., 2012).

Our SGD studies were carried out at four locations that span the coastline of Maunalua Bay: Black Point Beach, Wailupe Beach, Niu Beach, and Hawaiʻi Kai (Fig. 1c). Water samples for geochemical analysis (i.e., nutrients and trace metals) were collected at Black Point and Niu. Black Point is located at the western-most end of the Bay, downgradient from a large residential area that is built on the coastal plain. Wailupe and Niu are in the central region of the Bay, about 4 and 5.5 km of east of Black Point, respectively. They are adjacent to steep developed hillsides near the eastern cove where wave action is dampened compared to conditions at Black Point. Hawaiʻi Kai is about 9 km east of Black Point, at the far northeastern end of the Bay within a sheltered embayment.

Groundwater flow in Hawaiʻi is predominantly through volcanic rock aquifers (Tribble, 2008; Frans et al., 2012). Along the southern shore of Oʻahu, including the vicinity of Maunalua Bay, the volcanic aquifer is overlain by sedimentary fill that serves as a confining caprock (Fig. 2a). As a result, groundwater in this area is under artesian pressure. At Black Point and Niu, groundwater can be seen discharging through focused vent structures (i.e., submarine springs) (Fig. 2b) and through beach face seeps along the shoreline (Fig. 2c). At Wailupe, in addition to beach face seeps, there is a large submarine spring that focuses groundwater discharge at a site just seaward of low tide (Dimova et al., 2012).

### 3.2. Sample collection

Water samples were collected from Black Point and Niu Beach (Fig. 1) in 2009 on June 2 and June 3, respectively. Groundwater was accessed by inserting a stainless steel Solinst drive-point piezometer (50-mesh cylindrical filter screen within a 20 mm drive-point body) into the sand to a depth of at least 2 m. The piezometer was placed close to the high tide line at each site. A peristaltic pump was used to draw groundwater though an acid-cleaned Teflon sampling line coupled to C-flex tubing. Coastal seawater was concurrently collected adjacent to the temporary piezometer site through an acid-cleaned Teflon sampling line that extended beyond the low-tide line and was anchored to a cinderblock. At Black Point, groundwater and corresponding seawater samples were collected hourly for a 9-hour period (05:30 to 14:30) during a rising tide (−0.06 to +0.55 m). One surface water sample was also collected from a coastal spring at Black Point. At Niu, samples were collected hourly to bi-hourly for a 12.5-hour period (06:00 to 18:30), also during a rising tide (−0.07 to +0.61 m). Due to field logistics we were not able to sample during the falling tide. All times reported are local, based on the Hawaiʻi-Aleutian Time Zone.

A high-capacity Geotech 0.45 μm disposable filter capsule was used for *in situ* filtration. Unfiltered and filtered samples for total mercury (HgT) analysis were collected in trace metal clean Teflon bottles and placed on wet ice immediately after collection, then frozen within 12 h. Filtered water samples were also collected for nutrient and metal analyses (including nitrate + nitrite; ammonium, phosphate, silicate, barium, cesium, chromium, manganese, molybdenum, and vanadium). Time series ancillary parameters (i.e., salinity, temperature, dissolved oxygen, and pH) were measured using a calibrated YSI multi-parameter field probe.

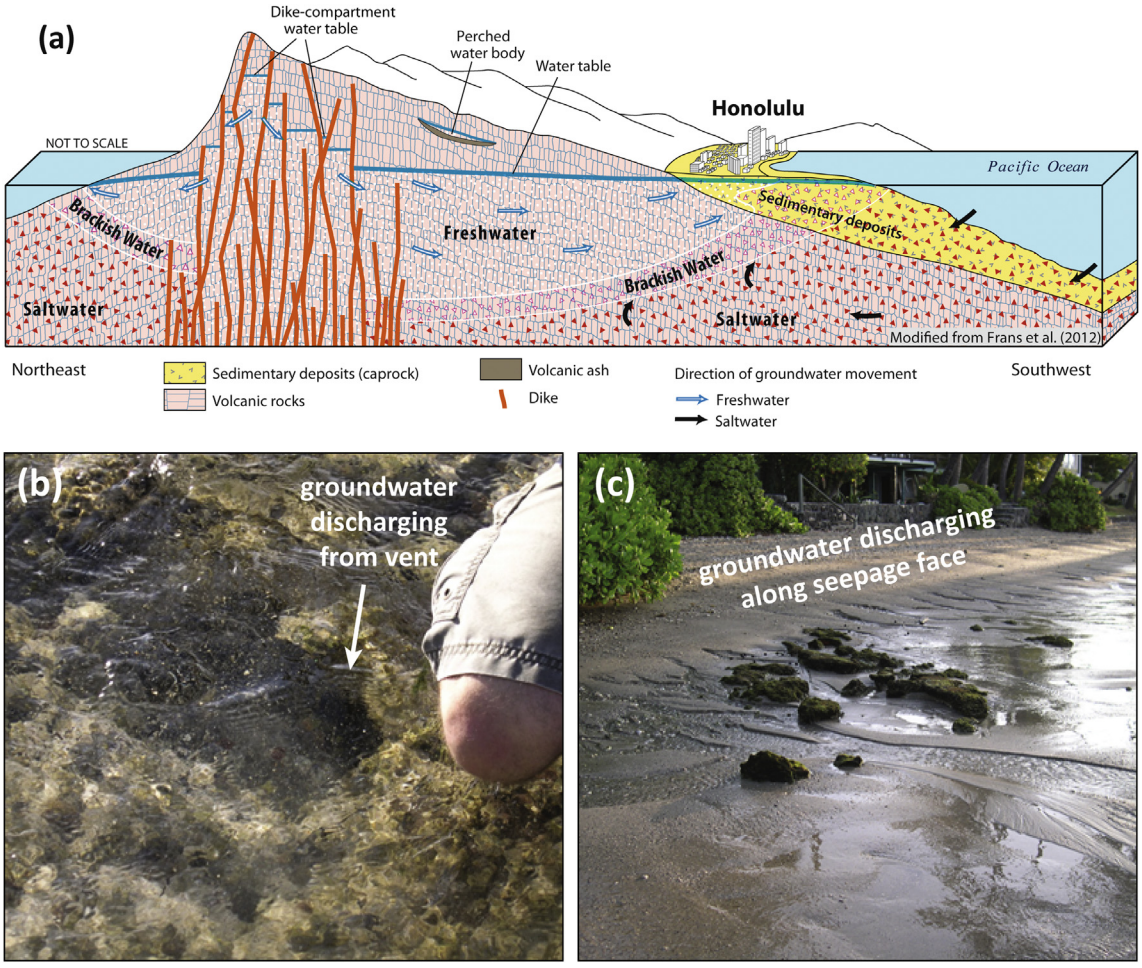


**Fig. 2.** (a) Schematic geologic cross section of Southern O'ahu showing groundwater–seawater interaction in the vicinity of Honolulu, HI (modified from Frans et al., 2012). Site photographs showing examples of (b) a groundwater vent discharging into nearshore seawater at Black Point (June 2, 2009, 10:30) and (c) groundwater seeps along the coastline of Niu (June 3, 2009, 09:30).

### 3.3. Sample analysis

Nutrient samples were analyzed using a Lachat Instruments QuickChem 8000 at Woods Hole Oceanographic Institution (WHOI), and metals (other than mercury) were analyzed on a HR-ICPMS at the University of Southern Mississippi. Methods for nutrient and trace metal analyses are outlined in Swarzenski et al. (2007).

All mercury samples were preserved and analyzed at the University of California, Santa Cruz (UCSC). Samples remained frozen until preservation, following protocols described by Parker and Bloom (2005). Samples were acidified while thawing to 0.5% (v/v) BrCl, and then stored in the dark at room temperature until analysis. HgT concentrations were determined by oxidation with BrCl, reduction with $SnCl_2$, gold trap amalgamation, and quantification by cold vapor atomic fluorescence spectrometry (CVAFS), based on established methods (Bloom and Crecelius, 1983; USEPA, 2002). The mean daily detection limit, calculated as three times the standard deviation of the laboratory blanks ($n = 16$), was 0.3 pM. Teflon bottles filled with Milli-Q® ultra-pure water (18.2 MΩ·cm at 25 °C) accompanied the sample bottles throughout field and laboratory procedures. HgT in these travel blanks ($n = 4$) was below the detection limit and analytically indistinguishable from laboratory blanks. The variability for samples analyzed more than three times was 0.5 ± 0.4 pM (mean ± one standard deviation, $n = 5$) and the mean percent difference for analytical duplicates was 23 ± 20% (mean ± one standard deviation; $n = 13$). The recovery for sample spikes was 94% and 97% ($n = 2$). Filtered and unfiltered field duplicates for seawater and groundwater were collected at Black Point (at time 09:30) and Niu (at time 12:00) (i.e., eight pairs of duplicate samples). The percent difference for filtered duplicates was 2.3 ± 2.9% ($n = 4$). The percent difference for unfiltered duplicates, excluding unfiltered groundwater from Black Point, was 2.8 ± 3.1% ($n = 3$). The HgT results for unfiltered duplicate groundwater samples at Black Point were 16 pM and 24 pM. These samples were collected when seawater infiltration was apparently rapid and we suspect sediment was entrained in our sampling line, resulting in sample variability (see Section 4.3.2).

### 3.4. Submarine groundwater discharge (SGD) measurements

We conducted field campaigns in November 2008 and in June 2009 to quantify rates and scales of SGD in Maunalua Bay using U/Th-series isotopic methods combined with electrical resistivity. Our general field approach consisted of strategically placed time series radon moorings as well as radon surveys in near-shore surface waters where we simultaneously conducted continuous resistivity profiling (CRP) surveys. A few land-based resistivity surveys were also conducted at specific sites of interest within Maunalua Bay. Groundwater radon, nutrients, and trace elements were collected

using shallow piezometers that were driven into nearshore sediment close to the high tide line while adjacent surface waters were collected for the same suite of analytes.

Rn-222 was first measured in the waters of Maunalua Bay to locate areas of enhanced coastal groundwater discharge. In mapping mode, three RAD7 $^{222}$Rn detectors were used in concert (Dulaiova et al., 2005) to obtain 'continuous' $^{222}$Rn activities along a shore-parallel transect that extended along the entire bay. The spatial resolution for $^{222}$Rn acquisition was a function of the boat speed, ambient radon activities, and the sampling interval of the RAD7 detectors. Briefly, seawater was pumped continuously from a depth of 0.5 m into an air/water exchanger that was plumbed into the RAD7s. The salinity and temperature as well as the boat's position was continuously recorded and later synchronized with the RAD7 output so that a map of $^{222}$Rn activities could be created. This map showed elevated radon activities (and associated salinity anomalies) at Black Point, Wailupe, Niu, and Hawai'i Kai, which were locations subsequently selected for detailed SGD assessments (Swarzenski et al., 2009).

Multi-day time-series measurements of bottom water $^{222}$Rn were obtained at Black Point and Niu using an anchored tender. Bottom water was continuously pumped into an air/water exchanger using a submersible pump. A single RAD7 detector was setup for 30-minute counting intervals. For each $^{222}$Rn time-series, a Solinst LTC Levelogger was deployed at the pump intake as well as on the seafloor; these instruments continuously measured pressure (water levels), conductivity (salinity), and temperature. The $^{222}$Rn and pressure data were then modeled using a transient box model to derive total (fresh + brackish) submarine groundwater discharge (SGD) rates following methods developed by Burnett et al. (2001), Burnett and Dulaiova (2003), and Burnett et al. (2006). We estimate a total measurement error of 30% on mean SGD values based on error propagation from calculated mixing losses, atmospheric evasion, and radon counting efficiencies. The range in SGD and HgT flux values reported in this paper represents the standard deviation of multiple $^{222}$Rn and HgT measurements made over the tidal period sampled, and not measurement errors.

To capture discharging groundwater at each site, a stainless-steel piezometer was installed to a depth greater than ~2 m just land-ward of the high tide line. Groundwater was continuously pumped from these piezometers and a CTD was used to assure that the groundwater discharge stream was not contaminated by ambient seawater. Time-series measurements of groundwater $^{222}$Rn were collected using these piezometers, and complimented with concurrent surface water samples collected in the adjacent seawater. Water-quality was continuously monitored and recorded using a calibrated YSI multi-parameter probe.

Multi-channel resistivity measurements were conducted in Maunalua Bay using two approaches: (1) marine (CRP) and (2) land-based (Swarzenski and Izbicki, 2009). CRP was first applied during $^{222}$Rn mapping, where a multi-electrode marine resistivity cable was also towed behind the survey boat. CRP-generated resistivity images generally corroborated enhanced groundwater flow at Black Point, Wailupe, and Niu. Land-based resistivity data was subsequently obtained at Wailupe using a 56-electrode resistivity cable connected to an external switching box routed to an AGI SuperSting multi-channel receiver. Time-series, land-based resistivity images collected at Wailupe were used to obtain independent submarine groundwater discharge rates at this site (Dimova et al., 2012).

## 4. Results and discussion

### 4.1. Submarine groundwater discharge (SGD)

At Black Point and Niu, $^{222}$Rn concentrations in seawater corresponded closely to tidal fluctuations (Fig. 3). The maximum $^{222}$Rn concentrations at Black Point coincided with extreme low tide (Fig. 3a), where the $^{222}$Rn peak at Niu typically lagged behind low tide (Fig. 3c). The average SGD flux based on a 4–5 day monitoring

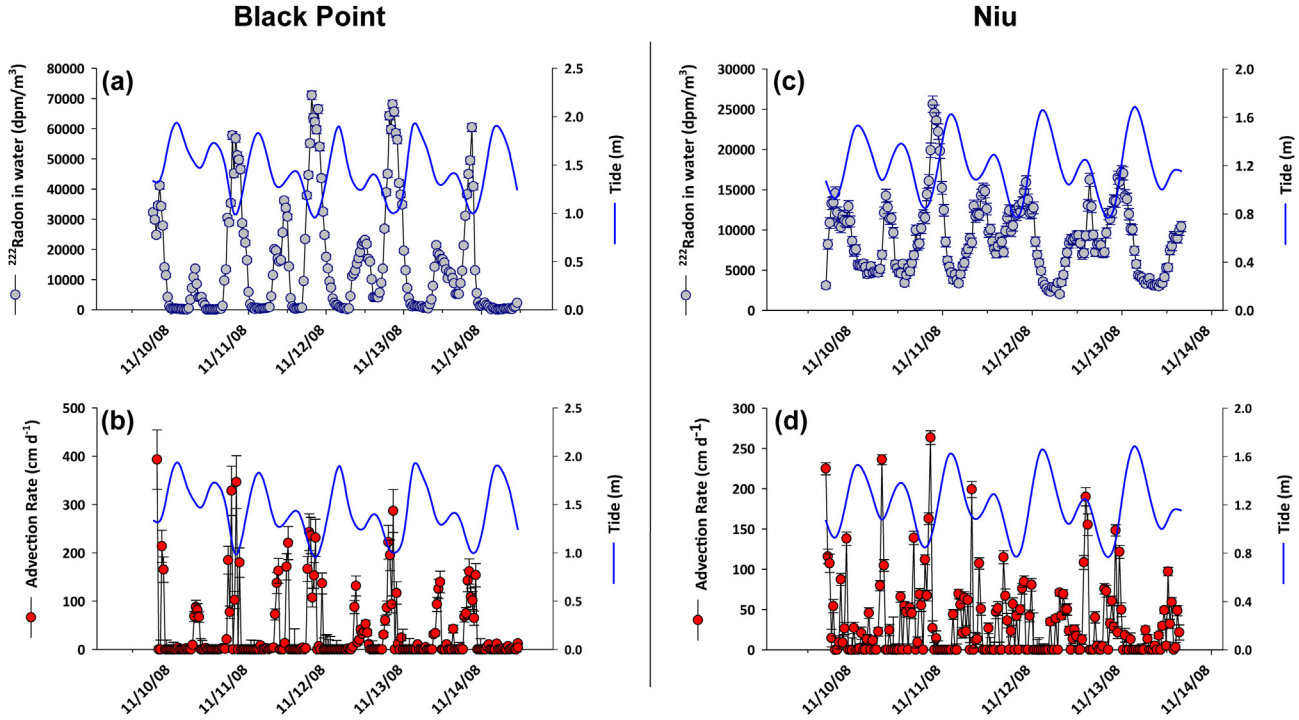


**Fig. 3.** Radon ($^{222}$Rn) measurements and associated groundwater advection rates from the Black Point (a and b) and Niu (c and d) sampling locations (November 9–14, 2008; Swarzenski et al., 2013).

**Table 1**
(a) Site specific and Maunalua Bay submarine groundwater discharge (SGD) estimates, (b) site specific and combined filtered (<0.45 μm) total mercury (F-HgT) concentrations in groundwater (GW) and seawater, and (c) site specific and Bay-wide HgT flux estimates. Table 1c presents the range of HgT flux results possible if calculations are made using the following concentration values for F-HgT in groundwater: 1) average over the period sampled; 2) average low tide; 3) average high tide; 4) minimum; 5) maximum. Comparison HgT concentration and flux values for sources other than SGD are shown in italics.

| | Black Point | Niu | Wailupe | Hawai'i Kai | Combined |
|---|---|---|---|---|---|
| a) Submarine groundwater discharge (SGD) flux estimates (units in $m^3\ m^{-2}\ d^{-1}$ unless specified)[*] | | | | | |
| $^{222}$Rn (Avg) | 0.602 ± 1.26 | 0.321 ± 0.483 | – | 0.168 ± 0.232 | 0.364 ± 0.456 |
| Elec Res | – | – | 0.91 ± 1.4[†] | – | 0.91 ± 1.4 |
| SGD Zones[‡] | WEST | CENTRAL (Niu & Wailupe) | | EAST | |
| | 0.602 ± 1.26 | 0.61 ± 0.72 | | 0.168 ± 0.232 | 0.46 ± 0.45[§] |
| Shoreline Contribution | 2600 m | 3600 m | | 3300 m | 9500 m |
| Maunalua Bay SGD Flux (assumed SGD zone of 9500 m × 100 m) | | | | | $4.3 \pm 4.3 \times 10^5\ m^3\ d^{-1}$ |
| b) Filtered HgT in coastal groundwater (GW) and seawater (units in pM, equivalent to nmol $m^{-3}$)[*] | | | | | |
| GW Average | 5.2 ± 2.0 | 3.4 ± 0.5[¶] | – | – | 4.3 ± 1.7 |
| GW Low Tide[‖] | 4.0 ± 0.8 | 3.7 ± 0.5[¶] | – | – | 3.9 ± 0.7 |
| GW High Tide[‖] | 6.7 ± 2.1 | 3.6 ± 0.3[¶] | – | – | 5.4 ± 2.3 |
| *Seawater* | *2.5 ± 0.2* | *1.5 ± 0.4* | – | – | *2.0 ± 0.7* |
| *North Pacific Surface Water (<40°N)* (Sunderland et al., 2009) | | | | | *1.02 ± 0.39* |
| c) SGD F-HgT flux estimates over a range of tidal conditions (units in nmol $m^{-2}\ d^{-1}$ unless specified)[*,**] | | | | | |
| Average | 3.1 ± 6.7 | 1.1 ± 1.7 | – | – | 2.0 ± 1.9 |
| Low Tide[‖] | 2.4 ± 5.1 | 1.2 ± 1.8 | – | – | 1.8 ± 1.7 |
| High Tide[‖] | 4.1 ± 8.6 | 1.1 ± 1.7 | – | – | 2.4 ± 2.5 |
| Calculated flux using minimum F-HgT (2.5 pM) | | | | | 1.1 ± 1.1 |
| Calculated flux using maximum F-HgT (8.8 pM) | | | | | 4.0 ± 3.9 |
| Maunalua Bay SGD HgT Flux using average F-HgT (4.3 ± 1.7 pM) | | | | | 0.68 ± 0.67 mol $yr^{-1}$ |
| *Atmospheric Deposition Estimate near Hawai'i* (Costa et al., 2012) | | | | | *0.2* |

[*] Range in $^{222}$Rn and HgT data represents variability due to tidal modulation (not measurement error).
[**] SGD F-HgT flux estimates determined by applying the specified groundwater F-HgT concentration (i.e., average, low tide, high tide, min, max) to each SGD zone and calculating a weighted average based on proportional shoreline contribution.
[†] Data from Dimova et al. (2012). SGD variability not reported; tidal conditions assumed to be similar to Niu and variability estimated as ±150% in calculations.
[‡] SGD zones were delineated from a shore-parallel map of $^{222}$Rn activities (see Section 4.1).
[§] Maunalua Bay-wide SGD flux determined by weighting the flux from each zone by its proportional shoreline contribution.
[¶] Average F-HgT value for Niu includes measurements made after high tide (falling limb); low and high tide concentrations only include rising limb F-HgT data, comparable to conditions at Black Point.
[‖] Approximate range in tidal elevation: low tide (−0.06 to +0.3 m); high tide (+0.3 to +0.6 m).

period was 0.602 ± 1.26 $m^3\ m^{-2}\ d^{-1}$ (60.2 ± 126 cm $d^{-1}$; $n = 227$) at Black Point and 0.321 ± 0.483 $m^3\ m^{-2}\ d^{-1}$ (32.1 ± 48.3 cm $d^{-1}$; $n = 190$) at Niu. At Hawai'i Kai, on the sheltered far northeastern end of Maunalua Bay, the average SGD flux was 0.168 ± 0.233 $m^3\ m^{-2}\ d^{-1}$ (16.8 ± 23.3 cm $d^{-1}$; $n = 163$), much lower than at the other sites. The reported range in these flux values represents variation due to tidal modulation, not measurement error (see Section 3.4).

Electrical resistivity images from Dimova et al. (2012) indicated that SGD at Wailupe was tidally modulated – the lens of submarine groundwater extended further offshore during low tide with a corresponding increase in SGD rates. The subsurface images also suggested that groundwater discharged from submarine vent structures as well as from diffusive seeps. These results were substantiated by visual observations of freshwater discharging from nearshore vents and seeps (e.g., Fig. 2b and c), with more intense flow occurring during low tide conditions. The SGD flux at Wailupe was estimated as 5900 $m^3\ d^{-1}$ per 65 m offshore extent based on salinity changes documented in the electrical resistivity images (the range in SGD due to tidal modulation was not reported in this study). This flux equates to approximately 0.91 $m^3\ m^{-2}\ d^{-1}$ assuming a 100 m lateral shoreline distance. Wailupe is about 2 km west of Niu in the same hydrogeological setting as our water sampling locations; therefore the results are considered applicable to our geochemical data set. For calculation purposes, we assumed the magnitude of tidal variability at Wailupe was similar to that at Niu (±150% based on multi-day $^{222}$Rn data) and report the Wailupe SGD flux as 0.91 ± 1.4 $m^3\ m^{-2}\ d^{-1}$ (Table 1).

The $^{222}$Rn and electrical resistivity flux estimates are similar in magnitude to values recently reported for Maunalua Bay (Black Point: 0.98 $m^3\ m^{-2}\ d^{-1}$ and Wailupe: 0.60 $m^3\ m^{-2}\ d^{-1}$, tidal variability not reported; Holleman, 2011; Dulaiova, 2013) and for other coastal sites in the Hawaiian Islands (Johnson et al., 2008; Peterson et al., 2009; Swarzenski et al., 2013). The $^{222}$Rn-derived estimates we made in November 2008 (Black Point, 0.602 ± 1.26 $m^3\ m^{-2}\ d^{-1}$; Niu, 0.321 ± 0.483 $m^3\ m^{-2}\ d^{-1}$; Hawai'i Kai, 0.168 ± 0.232 $m^3\ m^{-2}\ d^{-1}$) are lower than those calculated via electrical resistivity in October 2010 (Wailupe, 0.91 ± 1.4 $m^3\ m^{-2}\ d^{-1}$; Table 1), which may be attributed to site specific conditions combined with lower than normal rainfall in the year preceding the 2008 $^{222}$Rn measurements (Fig. 4; Wolanski et al., 2009; NOAA, 2013). The $^{222}$Rn SGD results demonstrate that groundwater discharge rates are consistently lower on the east side of the Bay. This observation is in agreement with the findings of Storlazzi et al. (2010), who reported that surface water salinity and circulation patterns in the eastern-most part of Maunalua Bay were distinct from other regions within the bay, despite similar inputs from coastal streams. They attributed this variability to a combination of factors, including the proximity of the marina at Hawai'i Kai and oceanographic influences from near-by Koko Head peninsula (Fig. 1).

We used the CRP shore-parallel map of $^{222}$Rn activities in Maunalua Bay (see Section 3.4) to delineate three SGD zones (western, central, and eastern) and calculated a weighted average SGD flux for the Bay (Swarzenski et al., 2009, 2013). Since SGD inputs are minimal along the eastern-most portion of the Bay, we assumed SGD occurred over 9.5 km of shoreline length rather than the entire ~12.5 km from Black Point to Koko Head. We applied the SGD rate from Black Point to the western zone (0.602 ± 1.26 $m^3\ m^{-2}\ d^{-1}$ over 2.6 km), the combined average SGD rate for Wailupe and Niu to the central zone (0.61 ± 0.72 $m^3\ m^{-2}\ d^{-1}$ over 3.6 km), and the SGD rate from Hawai'i Kai to the eastern zone (0.168 ± 0.232 $m^3\ m^{-2}\ d^{-1}$ over

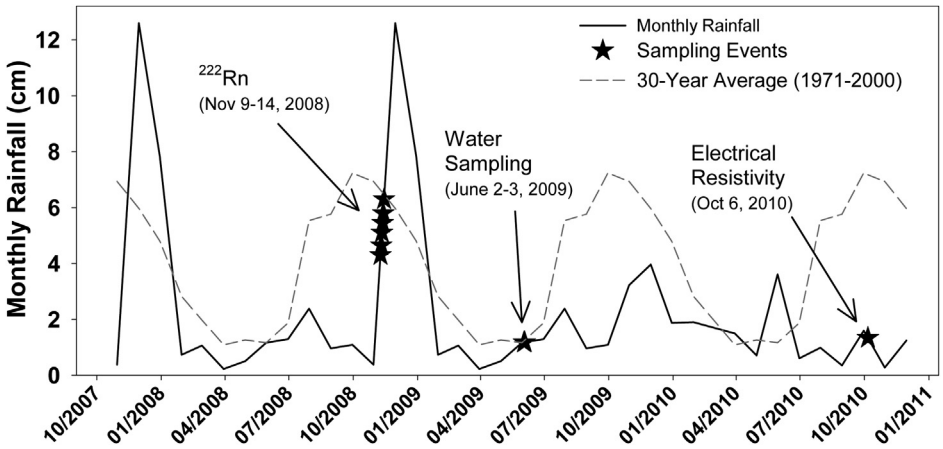


**Fig. 4.** Monthly rainfall in Honolulu, HI preceding the submarine groundwater discharge (SGD) measurements (2008 and 2010) and the water sampling event (2009). The annual average rainfall in Honolulu during 2008, 2009, and 2010 was 37 cm, 32 cm, and 44 cm, respectively. The 30-year annual average rainfall is 46 cm (NOAA, 2013).

3.3 km). Based on data from these SGD sampling locations, the weighted average groundwater flux along the Maunalua Bay coastline was approximately $0.46 \pm 0.45$ m$^3$ m$^{-2}$ d$^{-1}$ (Table 1). Data from the shore-parallel $^{222}$Rn activity map and resistivity images suggest SGD occurs over a ~100 m distance seaward from shoreline, resulting in a Bay-wide SGD zone of 0.95 km$^2$ and a groundwater flux estimate of $4.3 \pm 4.3 \times 10^5$ m$^3$ d$^{-1}$. Since we targeted areas with elevated $^{222}$Rn activities for this study, our Bay-wide SGD flux estimate may be biased toward higher fluxes and we consider this estimate an upper bound.

### 4.2. Geochemistry

Changes in surface water and groundwater geochemistry suggest that groundwater-seawater interaction in Maunalua Bay was influenced by tidal modulation. At Black Point, the geochemistry of nearshore groundwater reflected seawater infiltration into coastal sediment during rising tide conditions. During low tide, groundwater was brackish and maintained a salinity <8.5. As the tide rose, salinity steadily increased from 7 to >24 (Fig. 5a). The composition of groundwater with respect to some dissolved nutrients and trace elements (e.g., nitrogen, ammonium, cesium, chromium; see Supplementary Appendix) shifted toward the composition of seawater, providing complementary evidence that seawater intrusion at Black Point altered the geochemistry of shallow coastal groundwater (i.e., pore water). The low seawater salinity of 23 recorded at low rising tide followed by a steady salinity increase from 28 to 33 over the next several hours, suggests the period of maximum groundwater discharge occurred at low falling tide shortly before we began sampling. This interpretation is supported by the November 2008 $^{222}$Rn SGD study (Swarzenski et al., 2013), which recorded the highest SGD rates at Black Point during the falling limb and at low tide conditions (Fig. 3b). Throughout our sampling event, which occurred during a rising tide, the rate of SGD was too low to discernibly alter overlying seawater geochemistry.

Geochemical evidence from the Niu sampling location indicates groundwater–seawater interaction was remarkably different from that at Black Point, despite similar tidal conditions. Most notably, groundwater at Niu remained below a salinity of 1 throughout the entire 12.5-hour sampling period (Fig. 5e), demonstrating that seawater did not infiltrate coastal sediment in the vicinity of our beach piezometer. In contrast, we recorded simultaneous changes in a number of other parameters (e.g., salinity, temperature, mercury, nitrogen, ammonium, cesium, chromium) in seawater following low tide, which shifted the geochemistry of seawater toward that of groundwater (Figs. 5 and 6c, and Supplementary Index). Between 08:00 and 09:00 on the rising limb, seawater salinity dropped from 33 to 21 and cooled by ~1.5 °C. In most cases, recorded changes were abrupt and seawater characteristics immediately began returning to previous conditions. This pattern suggests a brief pulse of groundwater was released shortly after low tide. Furthermore, the November 2008 $^{222}$Rn SGD study consistently reported the maximum groundwater discharge rates after low tide (Fig. 3c; Swarzenski et al., 2013). Although the $^{222}$Rn measurements were made about 6-months before the water sampling event (June 2009), the response of groundwater to tidal fluctuations was expectedly similar. In summary, groundwater discharge at Niu was evidenced by changes in seawater geochemistry, whereas at Black Point seawater infiltration directly altered groundwater geochemistry.

### 4.3. Total mercury (HgT) concentrations in groundwater and seawater

#### 4.3.1. Black Point Beach seawater

The HgT concentration trends in filtered and unfiltered seawater at Black Point were notably different. Filtered HgT (F-HgT) concentrations were between 2 and 3 pM and varied little throughout the 9-hour sampling event despite changing tidal conditions (Fig. 6a). These values are similar to reported concentrations at several other SGD-HgT study sites (Black et al., 2009; Lee et al., 2011; Ganguli et al., 2012; Rahman et al., 2013), but on the low end of ranges typically found in urban impacted bays (e.g., Mason et al., 1999; Conaway et al., 2003; Fitzgerald et al., 2007). In North Pacific Ocean waters, F-HgT is ~1 pM (Sunderland et al., 2009) – slightly lower than filtered seawater in Maunalua Bay during our July sampling event.

In contrast to filtered seawater, unfiltered Hg-T (U-HgT) in seawater in Maunalua Bay changed substantially over time. During rising low tide, U-HgT at Black Point remained close to 6 pM, then steadily climbed to about 20 pM by high tide (Fig. 6a). We attribute this approximately three-fold increase to a rise in suspended particulate matter (SPM) in response to wave action as the tide came in (Fig. 7a). The SPM in Maunalua Bay is organic-rich and probably comprised largely of algal detritus (Wolanski et al., 2009). Mercury has a high affinity for organic matter (Lamborg et al., 2004) and is particle reactive (Fitzgerald et al., 2007; Conaway et al., 2008). Therefore, there is likely a positive correlation between mercury concentrations in unfiltered seawater in Maunalua Bay and the amount of particulate matter suspended in the water column.

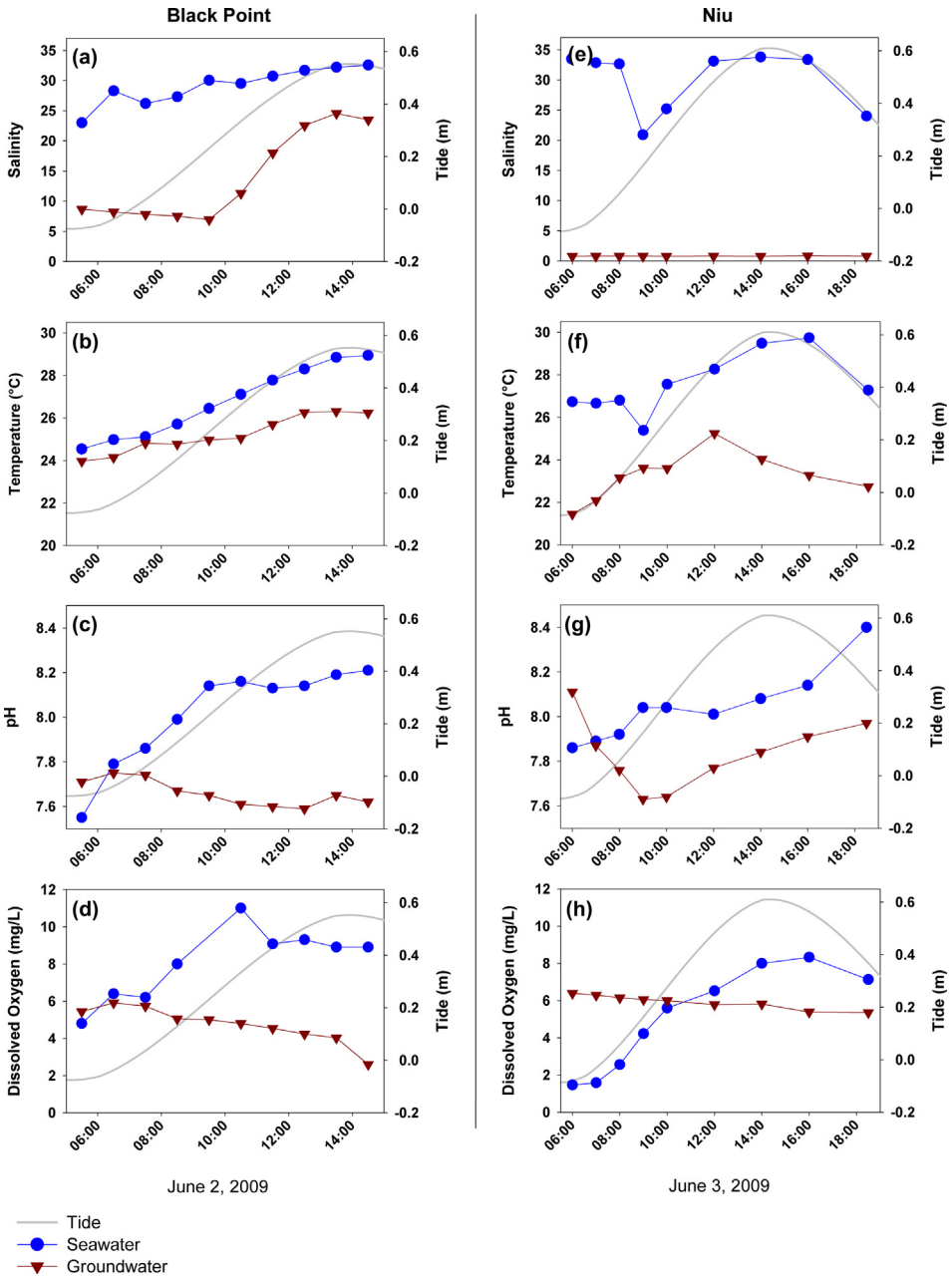


**Fig. 5.** Ancillary parameters (salinity, temperature, pH, and dissolved oxygen) in seawater (blue circles) and groundwater (red triangles) obtained at Black Point Beach (a–d), and Niu Beach (e–h) during a rising tide (solid gray line), June 2–3, 2009. (For interpretation of the references to color in this figure legend, the reader is referred to the web version of this article.)

Although we do not have direct SPM measurements from our 2009 sampling event, HgT trends in our data as well as turbidity and suspended sediment concentration (SSC) trends observed by other researchers (Wolanski et al., 2009; Storlazzi et al., 2010; Presto et al., 2012) support the premise that HgT concentrations in unfiltered seawater rose as a result of an increase in suspended particles. First, mercury concentrations at Black Point increased only in our unfiltered seawater samples; filtered concentrations remained stable regardless of changes in tide or wave action. Second, multiple long term monitoring studies (i.e., 4–6 months) in Maunalua Bay have recorded increased turbidity during high tide and in response to wave height (Wolanski et al., 2009; Storlazzi et al., 2010; Presto et al., 2012). Finally, turbidity in Maunalua Bay was reported to quickly return to initial conditions when the turbidity-triggering event ended (Storlazzi et al., 2010). This finding is consistent with our seawater U-HgT data – stable low concentrations over several hours during low tide followed by a rapid increase with the rising tide (Fig. 6a).

### 4.3.2. *Black Point Beach groundwater*

Groundwater U-HgT concentrations at Black Point were around 6–7 pM during low tide and doubled to about 14 pM by high tide (Fig. 6b). During low tide, we also sampled an intertidal groundwater-fed spring located at Black Point. Two of the unfiltered groundwater samples collected during the rising limb had notably higher concentrations (~20 and 24 pM), but were separated by a low concentration measurement (~8 pM) in the hour between; these anomalously high concentration measurements are

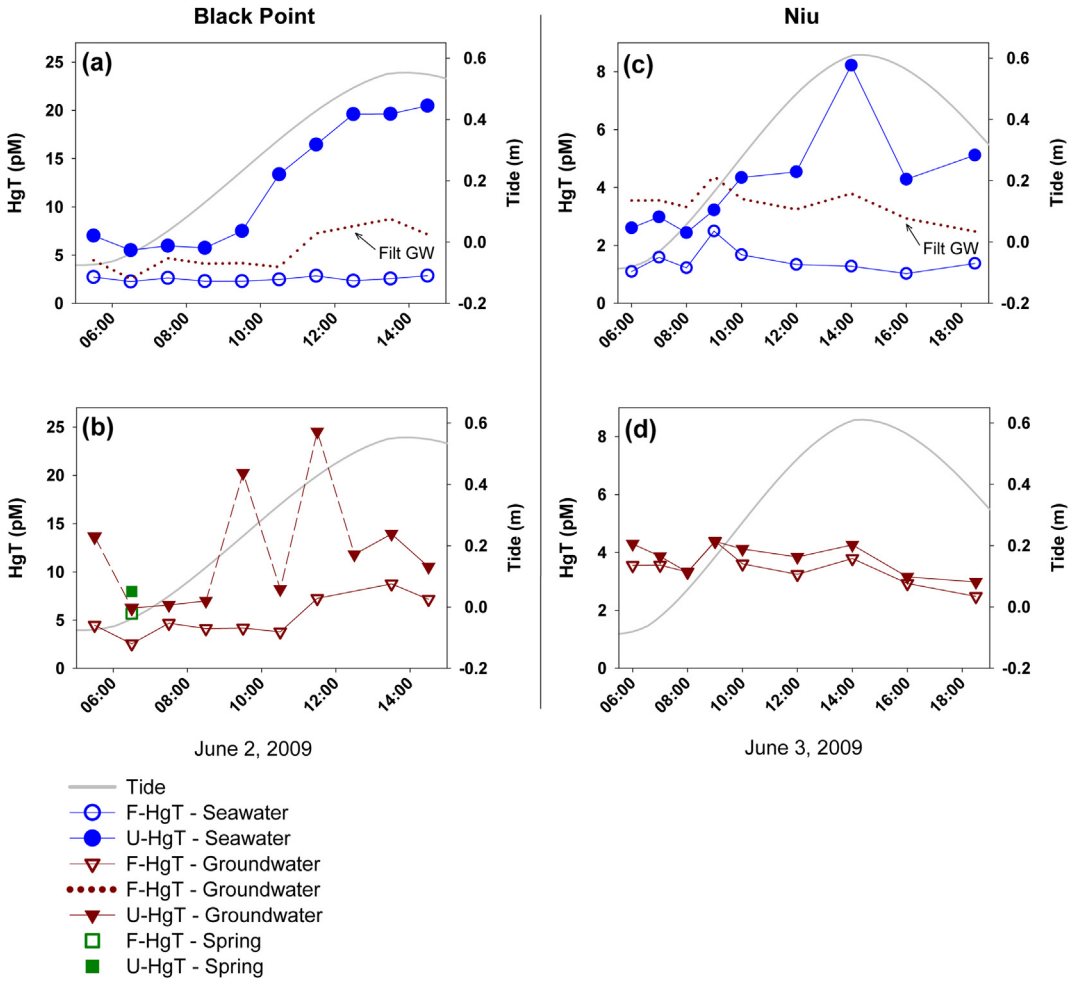


**Fig. 6.** Total mercury concentrations in filtered (<0.45 μm; F-HgT) and unfiltered (U-HgT) seawater (blue circles), groundwater from a depth ≥2 m (red triangles), and spring water (green squares) at Black Point Beach (a and b) and Niu Beach (c and d). Samples were collected during a rising tide (solid gray line). Unfiltered samples are shown as closed symbols and filtered samples are shown as open symbols. F-HgT in groundwater is also presented as a dotted black line on the seawater graphs. Note that the scale on the primary *y*-axis is different between the two sites. (For interpretation of the references to color in this figure legend, the reader is referred to the web version of this article.)

likely a result of entrained sediment and reflect the variability that can be inherent in unfiltered samples, especially in high energy systems. These samples were collected when groundwater salinity was changing most rapidly, rising from 7 to 18 in just 2 h (Fig. 5a). The rapid infiltration of seawater into coastal sediment combined with increasing tidal action could have dislodged and mobilized grains, enhancing the likelihood of particles entering our sample line. Excluding the two highest U-HgT values, which are outliers, the pattern of increasing concentrations in unfiltered groundwater roughly corresponds to the rising tide (Fig. 6b). Mercury concentrations in the intertidal spring water sample (F-HgT ~5.5 pM; U-HgT ~8 pM) were similar to those found in groundwater samples collected during the same time interval. This yields confidence that the temporary piezometer indeed captured representative coastal groundwater en route to the sea.

HgT in filtered groundwater mimicked the pattern observed in unfiltered groundwater (omitting the outliers), but remained consistently lower in concentration (Fig. 6b). The average F-HgT concentration at low tide was 4 pM and increased to almost 9 pM at high tide. If the anomalously high U-HgT data points are excluded, F-HgT concentrations remained roughly 4 pM below U-HgT throughout the tidal cycle (i.e., F-HgT and U-HgT concentrations increased by the same magnitude). Given this parallel, it appears mercury partitioning between the dissolved and particulate phase in groundwater was not measurably altered by seawater infiltration.

The concurrent increase in groundwater F-HgT and U-HgT concentrations may have been induced by flushing sediment pore space when seawater rapidly infiltrated the coastal aquifer, as illustrated in Fig. 7a. If pore water was in contact with sediment grains for several hours, it would likely have elevated F-HgT concentrations relative to groundwater that was continuously moving through the aquifer. Seawater infiltration at Black Point, which would primarily introduce dissolved constituents to groundwater, probably lessened the effect of pore water flushing because the F-HgT concentration in seawater was less than both F-HgT and U-HgT concentrations in groundwater (cf. Fig. 6a and b). Although U-HgT in seawater exceeded F-HgT and U-HgT concentrations in groundwater, it is improbable that particles suspended in seawater penetrated to the depth of the piezometer (≥2 m). Furthermore, an addition of particle-bound mercury would not cause the increase we observed in filtered groundwater HgT concentrations.

#### 4.3.3. Niu Beach seawater

Trends in seawater U-HgT at Niu were similar to those at Black Point (cf. Fig. 6a and c). The average U-HgT in seawater at Niu was close to 2.5 pM at low tide and reached a maximum of 8 pM at high tide. The elevated high tide concentrations were likely due to an

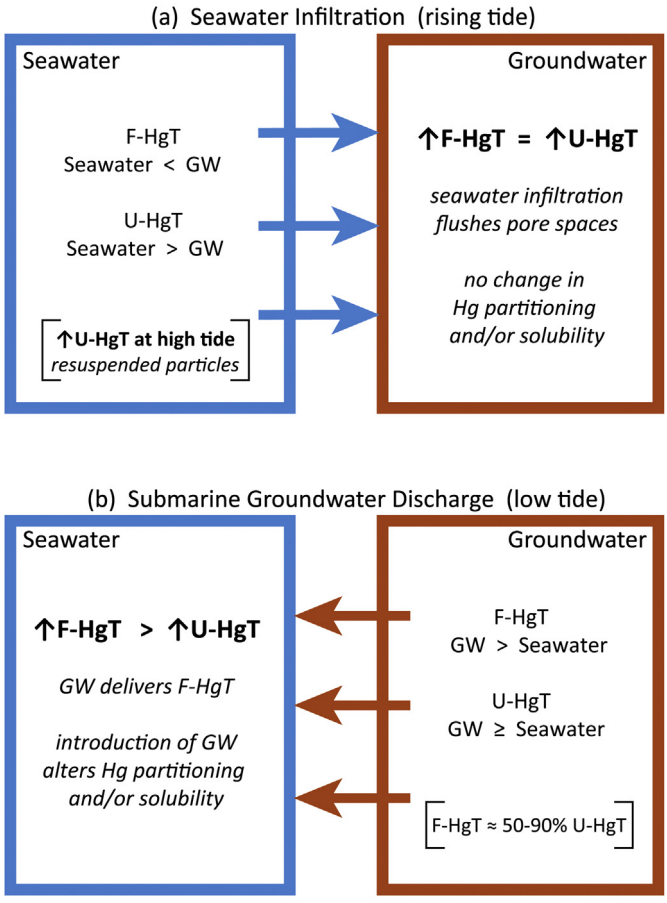


**Fig. 7.** Illustration of concentration trends in filtered total mercury (F-HgT) and unfiltered total mercury (U-HgT) in response to (a) seawater infiltration and (b) submarine groundwater discharge in Maunalua Bay, Hawai'i. Observed changes in concentration are shown in bold font and proposed physical and geochemical driving mechanisms are shown in italics.

increase in suspended particulates, as described in the Black Point Beach Seawater discussion (Section 4.3.1). The most notable difference between the Niu and Black Point sampling locations with respect to U-HgT in seawater was the range in concentrations. Seawater at Niu (U-HgT ~2.5–8 pM) spanned a narrower range than at Black Point (U-HgT ~6–20 pM). This difference is likely related to the concentration of suspended particulate matter in nearshore seawater in response to currents, wave action, and fetch. As previously noted, Niu is located in central Maunalua Bay, adjacent to a protective cove on the east side of the Bay (Fig. 1c). Conversely, Black Point is at the far west end of the Bay and is relatively unprotected (Section 3.1). In addition, during our sampling campaign, wave action at Niu was noticeably lower than at Black Point, which would likely result in lower SPM and therefore lower U-HgT concentrations.

The HgT concentration in filtered seawater at Niu was around 1.5 pM throughout most of our sampling event – approximately 1 pM less than concentrations observed at Black Point (cf. Fig. 6a and c). However, unlike F-HgT in seawater at Black Point which did not change over time, we recorded a concentration increase at Niu just after low tide, when the F-HgT concentration jumped to 2.5 pM. The timing of the change in filtered seawater was echoed in a number of other parameters (Fig. 5 and Supplementary Index ), indicating a shift in the geochemistry of seawater toward that of groundwater. As described in Section 4.2, we believe a pulse of groundwater mixed with seawater during that time interval. Therefore, the observed increase in seawater F-HgT at Niu was likely due in part to groundwater with a F-HgT concentration of ~4 pM discharging to seawater with a F-HgT concentration of ~1.5 pM (cf. Fig. 6c and d).

The observed mercury increase in the filtered fraction of seawater could have been augmented by a change in the partitioning of mercury in response to groundwater mixing (Fig. 7b). Prior to mixing with groundwater, F-HgT in seawater accounted for about 50% of the U-HgT (i.e., dissolved + particulate). When the pulse of groundwater was released, F-HgT in seawater comprised more than 75% of the U-HgT concentration. Additionally, the F-HgT concentration in seawater at Niu increased by 1.3 pM (1.2–2.4 pM) between 08:00 and 09:00, where the U-HgT only increased by 0.8 pM (2.5–3.2 pM) over the same time interval (Fig. 6c). If the addition of groundwater-derived F-HgT was the only factor driving this change in seawater, we would expect filtered and unfiltered HgT to increase by the same amount. Therefore, the larger HgT increase in filtered water relative to unfiltered water suggests solubility dynamics in seawater at Niu were altered due to groundwater–seawater interaction. This phenomena was not observed at Black Point, where seawater infiltration altered groundwater geochemistry (Section 4.3.2; cf. Fig. 7a and b).

Geochemical data from Niu indicate that almost all of the mercury in groundwater occurred in the filtered fraction (see Section 4.3.4 below). If the geochemistry of groundwater was such that mercury partitioning into the dissolved phase (i.e., <0.45 μm) was enhanced, then mercury solubility in seawater at Niu could have been affected by elevated SGD rates. The considerable drop in seawater salinity from 32 to 21 just after low tide (Fig. 5e), may also have altered mercury dynamics and demonstrates that although the groundwater pulse was brief, a substantial amount of groundwater was discharged. The coincidence of the groundwater pulse with the rising tide (which presumably caused a simultaneous increase in seawater SPM and U-HgT) makes it difficult to determine whether the increase in seawater F-Hg-T was due to SGD or a result of altering mercury solubility dynamics. Our data suggest both processes were in play at Niu (Fig. 7b).

#### 4.3.4. Niu Beach Groundwater

Filtered and unfiltered HgT concentrations in groundwater at Niu were almost identical, with F-HgT accounting for about 90% of the U-HgT concentration (Fig. 6d). Similar findings have been reported in other SGD studies, with higher than expected concentrations of dissolved mercury (i.e., <0.45 μm) relative to particulate mercury in coastal groundwater and seawater (Bone et al., 2007; Laurier et al., 2007; Black et al., 2009; Ganguli et al., 2012). We observed a general decreasing trend in HgT following low tide, with concentrations dropping from 4.3 to 3.0 pM. This decline was fairly constant over time.

The most notable change in groundwater mercury concentrations was a ~1 pM increase (3.3–4.4 pM) shortly after low tide, during the same interval we suspect groundwater discharge was greatest. It is possible this observed increase was a product of sample variability in a dynamic coastal setting. However, the timing corresponds to a shift in seawater geochemistry that we attribute to groundwater export from the aquifer (Section 4.3.3). Additionally, the partitioning of mercury between the dissolved and particulate phase appears to have changed during that sampling interval, with all mercury in groundwater occurring in the filtered phase (F-HgT = U-HgT; Fig. 6d). If this change in groundwater HgT was a result of physical processes, the concentration increase may reflect enhanced flushing of the pore space around grains if there was a surge in the SGD rate. Likewise, the gradual decrease in HgT concentrations following the surge in SGD may be due to reduced flushing of pore space as groundwater discharge declined during high tide.

### 4.4. Mercury loadings to Maunalua Bay

We determined the site specific groundwater flux of mercury to nearshore seawater at Black Point and Niu by multiplying each site's average groundwater F-HgT concentration (5.2 ± 2.0 pM and 3.4 ± 0.54 pM, respectively) by the mean $^{222}$Rn derived SGD rate (0.602 ± 1.26 $m^3$ $m^{-2}$ $d^{-1}$ and 0.321 ± 0.483 $m^3$ $m^{-2}$ $d^{-1}$, respectively; Table 1 and Fig. 8). We estimate the mercury flux was 3.1 ± 6.7 nmol $m^{-2}$ $d^{-1}$ at Black Point and 1.1 ± 1.7 nmol $m^{-2}$ $d^{-1}$ at Niu. We calculated a Maunalua bay-wide SGD mercury flux of 0.68 ± 0.67 mol $yr^{-1}$ (2.0 ± 1.9 nmol $m^{-2}$ $d^{-1}$ when normalized for surface area; Table 2) by applying the average F-HgT concentration in groundwater from Black Point and Niu (4.3 ± 1.7 pM) to each of the three SGD zones delineated by the CRP shore-parallel map of $^{222}$Rn activities (Section 4.1) and weighting each flux by its proportional shoreline distance. We combined groundwater F-HgT data from both Black Point and Niu for our Bay-wide flux calculation because there was insufficient data to define zones of mercury concentrations within the Maunalua Bay groundwater system. However, if we apply the groundwater F-HgT concentration from Black Point to the western SGD zone and the groundwater F-HgT concentration from Niu to the central and eastern SGD zones, we calculated a similar Bay-wide SGD mercury flux of 0.64 ± 0.72 mol $yr^{-1}$. Reported values for the annual atmospheric deposition of mercury in the vicinity of the Hawaiian Islands is approximately 0.2 nmol $m^{-2}$ $d^{-1}$ (Costa et al., 2012), about an order of magnitude lower than our estimates for SGD mercury inputs. Although we do not know the flux of mercury to Maunalua Bay due to surface water runoff, groundwater discharge appears to be an important component of the coastal mercury budget in this region (Table 1).

We consider the SGD and water sampling data sets compatible because precipitation was relatively similar in the months preceding all three field campaigns even though they occurred over a period of two years, from November 2008 to October 2010 (Fig. 4; NOAA, 2013).

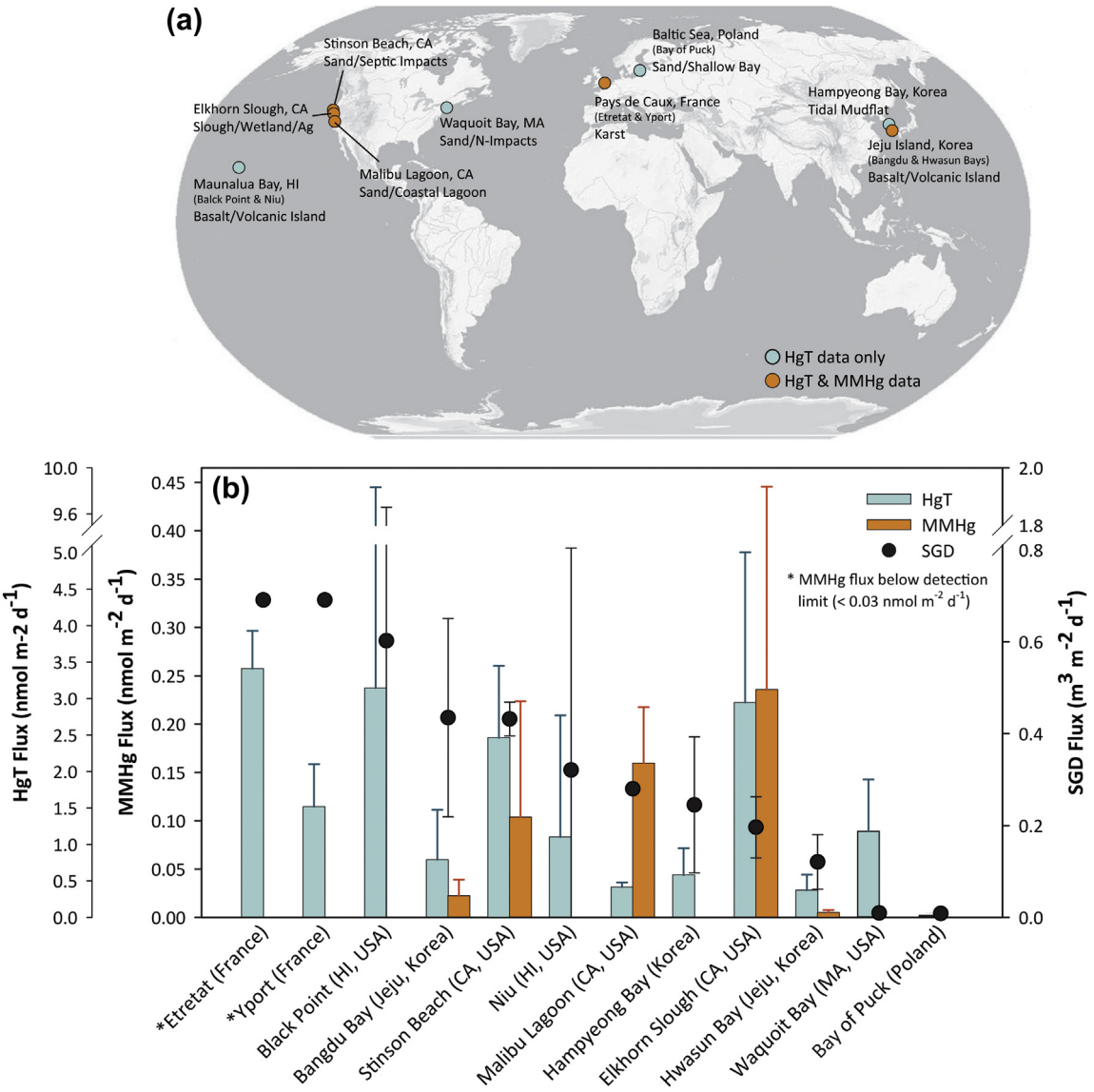


**Fig. 8.** (a) Map identifying locations where the flux of total mercury (HgT) associated with submarine groundwater discharge (SGD) has been quantified and (b) comparison of SGD (black dots), total mercury (HgT) (blue bars), and monomethylmercury (MMHg) (orange bars) flux estimates. Data are compiled from Bone et al., 2007 (Waquoit Bay), Laurier et al., 2007 (Etretat and Yport), Black et al., 2009 (Stinson Beach and Elkhorn Slough), Lee et al., 2011 (Bangdu Bay and Hwasun Bay), Ganguli et al., 2012 (Malibu Lagoon), Rahman et al., 2013 (Hampyeong Bay), and Szymczycha et al., 2013 (Bay of Puck). The observed variation in flux values is due to tidal modulation, not measurement error. (For interpretation of the references to color in this figure legend, the reader is referred to the web version of this article.)

**Table 2**
Comparison of submarine groundwater discharge (SGD) flux rates, filtered total mercury (F-HgT) concentrations in seawater (SW) and groundwater (GW), and bay-wide F-HgT flux estimates from locations where SGD-HgT studies have been conducted.

| Location | SGD Area ($km^2$) | SGD Flux ($km^3\ yr^{-1}$) | F-HgT SW* (pM, $mol/km^3$) | F-HgT GW* (pM, $mol/km^3$) | F-HgT Flux* ($mol\ yr^{-1}$) | F-HgT Flux* ($mol\ km^{-2}\ yr^{-1}$) | Reference |
|---|---|---|---|---|---|---|---|
| Bay of Puck (Baltic sea, Poland) | 9.8† | 0.03 | 22–32 | 3.1 ± 1.0 | 0.094 ± 0.031 | 0.0096 ± 0.0032 | Szymczycha et al. (2013) |
| Hwasun Bay (Jeju Island, Korea) | 1.7 | 0.075 ± 0.037 | 1.2–2.5 | 3.0 ± 1.0 | 0.23 ± 0.14 | 0.135 ± 0.079 | Lee et al. (2011) |
| Santa Monica Bay (Malibu, CA, USA) | 6† | 0.61 | 1.5 ± 0.99 | 1.5 ± 0.24 | 0.90 ± 0.15 | 0.15 ± 0.025 | Ganguli et al. (2012) |
| Hampyeong Bay (Yellow Sea, Korea) | 85 | 7.6 ± 4.6 | 0.83–2.0 | 2.4 ± 0.5 | 18 ± 12 | 0.21 ± 0.14 | Rahman et al. (2013) |
| Bangdu Bay (Jeju Island, Korea) | 0.80 | 0.127 ± 0.063 | 1.2–1.5 | 1.8 ± 1.3 | 0.23 ± 0.20 | 0.29 ± 0.25 | Lee et al. (2011) |
| Waquoit Bay (MA, USA) | 3.9† | 0.014 | 18–256 | 50–200‡ | 0.68–2.7 | 0.17–0.69 | Bone et al. (2007) |
| Maunalua Bay (HI, USA) | 0.95§ | 0.16 ± 0.16 | 2.0 ± 0.65 | 4.3 ± 1.7 | 0.68 ± 0.67 | 0.72 ± 0.71 | This study |
| Bolinas Bay (Stinson Beach, CA, USA) | 0.80§ | 0.13 ± 0.01 | 1.7–2.6 | 5.7 ± 3.2 | 0.7 ± 0.3 | 0.90 ± 0.36 | Black et al. (2009) |
| Pays de Caux Region¶ (Seine Estuary, France) | 10§ | 2.5 | 3.6 ± 1.0 | 3.6 ± 0.57 | 9.0 ± 1.4 | 0.90 ± 0.14 | Laurier et al. (2007) |
| Elkhorn Slough (Central CA, USA) | 2.7 | 0.19 ± 0.07 | 0.8–11.6 | 15 ± 9.0 | 2.9 ± 2.0 | 1.1 ± 0.75 | Black et al. (2009) |

* Concentration and flux values separated by a dash (–) represent the reported range.
† Calculations for SGD area values described in the Supplementary Index.
‡ Authors report a range of <3.2–262 pM in groundwater, but use an average range of 50–200 pM for SGD-HgT flux calculations.
§ Area determined by estimating shoreline distance along the bay and assuming a 0.1 km wide SGD zone.
¶ (1) Pays de Caux is a karstic region within the Seine Estuary – values do not represent the entire estuary. (2) Concentration and F-HgT fluxes estimates were determined by averaging values from Etretat and Yport.

The average annual rainfall in the Honolulu area is 46 cm with the majority of precipitation occurring between November and January (Wolanski et al., 2009; NOAA, 2013). All of our sampling events preceded the rainy season and there was only about 2 cm of accumulated rainfall in the ~35 days before each sampling event. One rain event began at the end of the November 2008 $^{222}Rn$ study (Fig. 4), but it did not appear to affect coastal groundwater discharge rates (Fig. 3).

We summarized the SGD flux ($km^3\ yr^{-1}$) and associated F-HgT flux ($mmol\ km^{-2}\ yr^{-1}$) estimates from ten bays around the world to place our results from Maunalua Bay into a broader context (Table 2). A description of our calculations and assumptions is included in the Supplementary Appendix. The lowest SGD flux of mercury ($0.0096 \pm 0.0032\ mol\ km^{-2}\ yr^{-1}$) was reported at the Bay of Puck in the Baltic Sea, Poland, where groundwater discharge with a F-HgT concentration of 3.1 ± 1.0 pM appeared to dilute HgT concentrations in the overlying seawater (F-HgT > 20 pM) (Szymczycha et al., 2013). We calculated an area-normalized mean mercury flux between ~0.1 and 0.3 $mol\ km^{-2}\ yr^{-1}$ for four of the ten bays evaluated, and a notably higher flux of ~0.7–1 $mol\ km^{-2}\ yr^{-1}$ at four other locations, including Maunalua Bay ($0.72 \pm 0.71\ mol\ km^{-2}\ yr^{-1}$). When surface area was taken into account, regions with larger SGD zones typically contributed more mercury to coastal seawater, with the highest F-HgT groundwater flux ($18 \pm 12\ mol\ yr^{-1}$) reported at Hampyeong Bay in the Yellow Sea along the coast of Korea, which has an SGD zone of approximately 85 $km^2$ (Table 2; Rahman et al., 2013). However, areas with high SGD rates, such as the karstic shoreline in the Pays de Caux Region of France (SGD flux = 2.5 $km^3\ yr^{-1}$), can also export relatively large quantities of mercury to nearshore seawater (F-HgT flux = $9.0 \pm 2.9\ mol\ yr^{-1}$) compared to sites with similar SGD zones and F-HgT concentrations, but with lower SGD rates (e.g., Bay of Puck; Laurier et al., 2007; Szymczycha et al., 2013). Maunalua Bay's SGD zone (0.95 $km^2$) was slightly smaller than most of the comparison bays, but it had an intermediate SGD flux and groundwater F-HgT concentration ($0.16 \pm 0.16\ km^3\ yr^{-1}$ and 4.3 ± 1.7 pM, respectively), resulting in a mercury flux of $0.68 \pm 0.67\ mol\ yr^{-1}$. However, broader SGD sampling coverage within each bay and a quantitative assessment of the area over which SGD rates can be applied are needed to draw more robust comparisons among coastal bays and estuaries.

### 4.5. Implications for monomethylmercury (MMHg) production in Maunalua Bay

While there are no MMHg data for Maunalua Bay, water circulation patterns, trends in dissolved oxygen (DO), and food web dynamics suggest MMHg production and biologic uptake should be evaluated. The residence time of water in the western portion of Maunalua Bay is less than a day; however, on the eastern side, sedimentation and physical modifications have increased the residence time of water to about a week (Wolanski et al., 2009; Storlazzi et al., 2010). As a result of the longer residence time and lower wave action, a permanent nepheloid layer comprised mainly of organic matter (possibly detritus from algal mats) develops in the water column of the east Bay during the dry season (Wolanski et al., 2009).

Water quality is further degraded by nutrient inputs from streams and groundwater discharge which can induce algal growth and eutrophication (Hoover and Mackenzie, 2009; Wolanski et al., 2009; Swarzenski et al., 2013). We observed a strong diurnal signal in seawater DO concentrations, which were low in the morning and increased throughout the afternoon (Fig. 5d and h). This trend is presumably due to algal respiration (DO drawdown) at night and photosynthesis (DO increase) during the day. DO drawdown was more pronounced at Niu, our central Bay site, where the water was shallower and warmer relative to Black Point (Fig. 5b and f). Other researchers have reported similar DO patterns in Maunalua Bay (Wolanski et al., 2009) as well as in other productive coastal waters of Hawai'i (e.g., Kāne'ohe Bay in O'ahu, Martinez et al., 2012). We also recorded a steady decline in DO (from 6 to 2 mg/L) in groundwater at Black Point over the course of our sampling period (Fig. 5d). Since anaerobic bacteria are largely responsible for converting inorganic mercury to bioaccumulative MMHg (Fitzgerald et al., 2007; Hu et al., 2013; Parks et al., 2013) zones of low DO

may provide a habitat conducive to MMHg production in the Bay. Furthermore, microbial activity might be amplified by the warm coastal waters of Maunalua Bay which ranged between ~25 and 32 °C during our sampling event (Fig. 5b and f).

The biological uptake of MMHg is also influenced by food web dynamics. Coral reef ecosystems, such as Maunalua Bay, typically have high rates of primary production and complex trophic connections compared to other marine environments (Grigg et al., 1984). Primary producers are the main entry point for MMHg into the base of aquatic food webs (Mason et al., 1996; Pickhardt and Fisher, 2007; Luengen and Flegal, 2009) and MMHg biomagnification may be enhanced by trophic complexity (Morel et al., 1998; Davis et al., 2003). Although an array of factors influence MMHg biomagnification in aquatic habitats (Lavoie et al., 2013), the trophic structure, water quality, and water circulation patterns in Maunalua Bay suggest future studies to evaluate mercury biogeochemical cycling in this ecosystem are warranted.

## 5. Conclusions

As more SGD-associated mercury flux data become available, we can begin to compare and contrast results from a range of locations. This will permit a more synoptic evaluation of the underlying controls on SGD and SGD-associated mercury transformations and fluxes. Such data are vital in terms of ecosystem health monitoring and management. The variability in data among and within systems is evident in Fig. 8, which presents published site-specific mercury flux values. Groundwater at Pays de Caux, France (Laurier et al., 2007), a karst system, has one of the highest discharge rates, along with Black Point in the Hawaiian Islands, where groundwater discharges through focused SGD vents and seeps (Fig. 2b and c). However, Niu, Hawai'i, as well as two sites on Jeju Island, Korea (Lee et al., 2011) have lower to moderate SGD rates despite both being volcanic in substrate. With respect to mercury flux, we discern no obvious trends, even among sites in the same hydrographic setting (e.g., Hawai'i, USA; Pays de Caux, France; Jeju Island, Korea), which suggests that the local geologic setting controls mercury concentrations and SGD rates, and so has a strong influence on mercury fluxes.

Given the continually changing dynamics of coastal environments over environmentally relevant time scales and distances, the variability among reported data is not surprising. Estimating groundwater discharge rates in these heterogeneous systems is compounded by the inherent range in SGD measurements which can vary by more than ±100% due to tidal modulation. However, the existing data provide insight into biogeochemical processes that occur at the land–sea interface. For example, there is growing evidence that groundwater–seawater interactions affect mercury partitioning and/or solubility dynamics in some locations (Bone et al., 2007; Laurier et al., 2007; Black et al., 2009; Ganguli et al., 2012). Additionally, MMHg production in coastal sediment may be a source of bioaccumulative mercury to nearshore seawater (Ganguli et al., 2012). Given our current understanding of SGD-mercury dynamics, we can develop sampling strategies specifically designed to evaluate some of these preliminary findings.

## Acknowledgments

This work could not have been accomplished without the expert help of many, including Gordon Tribble (USGS-Honolulu), Natasha Dimova (UA-Tuscaloosa), Sarah Rosa (USGS-Honolulu), Jacque Kelly (Georgia Southern University), Carrie Plath (UH-Manoa), Christopher Conaway (USGS-Menlo Park), Carl Lamborg (WHOI), and members of the WIGS Lab (UC Santa Cruz). We are very grateful for the help and logistical support of Mālama Maunalua, particularly to Alyssa Miller and Carol Wilcox. We are indebted to John Haines of the USGS Coastal and Marine Geology Program for sustained support in coastal aquifer science. We also appreciate the insightful and constructive input we received from the anonymous reviewers. This work was sponsored in part by the University of Hawaii Sea Grant College Program under Institutional Grant No. NA09OAR4170060 [UNIHI-SEAGRANT-JC-09-56]. The analytical component of this project was supported with funds from the Robert & Patricia Switzer Foundation, the University of California Toxic Substances Research & Teaching Program (UC TSR&TP), the Friends of Long Marine Laboratory (FLML), and the Dr. Earl H. Myers and Ethel M. Myers Oceanographic and Marine Biology Trust. The use of trade names is for descriptive purposes only and does not imply endorsement by the U.S. Government.

## Appendix A. Supplementary data

Supplementary data related to this article can be found at http://dx.doi.org/10.1016/j.ecss.2014.01.012.

## References

Benoit, J., Gilmour, C.C., Heyes, A., Mason, R.P., Miller, C.L., 2003. Geochemical and biological controls over methylmercury production and degradation in aquatic ecosystems. In: Cai, Y., Braids, O.C. (Eds.), Biogeochemistry of Environmentally Important Trace Elements. American Chemical Society, Washington DC, pp. 262–297.

Black, F.J., Paytan, A., Knee, K.L., De Sieyes, N.R., Ganguli, P.M., Gary, E., Flegal, A.R., 2009. Submarine groundwater discharge of total mercury and monomethylmercury to Central California coastal waters. Environ. Sci. Technol. 43, 5652–5659.

Bloom, N.S., Crecelius, E.A., 1983. Determination of mercury in seawater at subnanogram per liter levels. Mar. Chem. 14, 49–59.

Blum, J.D., Popp, B.N., Drazen, J.C., Anela Choy, C., Johnson, M.W., 2013. Methylmercury production below the mixed layer in the North Pacific Ocean. Nat. Geosci. 6, 879–884.

Bone, S.E., Charette, M.A., Lamborg, C.H., Gonneea, M.E., 2007. Has submarine groundwater discharge been overlooked as a source of mercury to coastal waters? Environ. Sci. Technol. 41, 3090–3095.

Burnett, W.C., Aggarwal, P.K., Aureli, A., Bokuniewicz, H., Cable, J.E., Charette, M.A., Kontar, E., Krupa, S., Kulkarni, K.M., Loveless, A., Moore, W.S., Oberdorfer, J.A., Oliveira, J., Ozyurt, N., Povinec, P., Privitera, A.M.G., Rajar, R., Ramassur, R.T., Scholten, J., Stieglitz, T., Taniguchi, M., Turner, J.V., 2006. Quantifying submarine groundwater discharge in the coastal zone via multiple methods. Sci. Total Environ. 367, 498–543.

Burnett, W.C., Dulaiova, H., 2003. Estimating the dynamics of groundwater input into the coastal zone via continuous radon-222 measurements. J. Environ. Radioact. 69, 21–35.

Burnett, W.C., Taniguchi, M., Oberdorfer, J., 2001. Measurement and significance of the direct discharge of groundwater into the coastal zone. J. Sea Res. 46, 109–116.

Conaway, C.H., Black, F.J., Grieb, T.M., Roy, S., Flegal, A.R., 2008. In: Whitacre, D.M. (Ed.), Mercury in the San Francisco Estuary, Rev. Environ. Contam. Toxicol., pp. 29–54.

Conaway, C.H., Squire, S., Mason, R.P., Flegal, A.R., 2003. Mercury speciation in the San Francisco Bay estuary. Mar. Chem. 80, 199–225.

Costa, M.F., Landing, W.M., Kehrig, H.A., Barletta, M., Holmes, C.D., Barrocas, P.R., Evers, D.C., Buck, D.G., Claudia Vasconcellos, A., Hacon, S.S., Moreira, J.C., Malm, O., 2012. Mercury in tropical and subtropical coastal environments. Environ. Res. 119, 88–100.

Davis, J.A., Yee, D., Collins, J.N., Schwarzbach, S.E., Luoma, S.N., 2003. Potential for increased mercury accumulation in the estuary food web. San. Francisco Estuary Watershed Sci. 1, 38.

Dimova, N.T., Swarzenski, P.W., Dulaiova, H., Glenn, C.R., 2012. Utilizing multichannel electrical resistivity methods to examine the dynamics of the fresh water–seawater interface in two Hawaiian groundwater systems. JGR 117, 12.

Dulaiova, H., 2013. Personal Communication, Assistant Professor. University of Hawaii.

Dulaiova, H., Peterson, R., Burnett, W., Lane-Smith, D., 2005. A multi-detector continuous monitor for assessment of $^{222}$R in the coastal ocean. J. Radioanal. Nucl. Chem. 263, 361–363.

Fitzgerald, W.F., Lamborg, C.H., Hammerschmidt, C.R., 2007. Marine biogeochemical cycling of mercury. Chem. Rev. 107, 641–662.

Frans, L.M., Rupert, M.G., Hunt Jr., C.D., Skinner, K.D., 2012. Groundwater Quality in the Columbia Plateau, Snake River Plain, and Oahu Basaltic-rock and Basin-Fill Aquifers in the Northwestern United States and Hawaii, 1992–2010. US Geological Survey Scientific Investigations Report 2012–5123.

Ganguli, P.M., Conaway, C.H., Swarzenski, P.W., Izbicki, J.A., Flegal, A.R., 2012. Mercury speciation and transport via submarine groundwater discharge at a southern California coastal lagoon system. Environ. Sci. Technol. 46, 1480–1488.
Grigg, R.W., Polovina, J.J., Atkinson, M.J., 1984. Model of a coral reef ecosystem. Coral Reefs 3, 23–27.
Holleman, K.D., 2011. Impact of Flux, Residence Time and Nutrient Load of Submarine Groundwater Discharge on Coastal Phytoplankton Growth in Coastal Waters of Hawai'i. Master's Thesis in Geology and Geophysics. University of Hawai'i, Manoa.
Hoover, D., Mackenzie, F., 2009. Fluvial fluxes of water, suspended particulate matter, and nutrients and potential impacts on tropical coastal water biogeochemistry: Oahu, Hawai'i. Aquat. Geochem. 15, 547–570.
Hu, H., Lin, H., Zheng, W., Tomanicek, S.J., Johs, A., Feng, X., Elias, D.A., Liang, L., Gu, B., 2013. Oxidation and methylation of dissolved elemental mercury by anaerobic bacteria. Nat. Geosci. 6, 751–754.
Johnson, A.G., Glenn, C.R., Burnett, W.C., Peterson, R.N., Lucey, P.G., 2008. Aerial infrared imaging reveals large nutrient-rich groundwater inputs to the ocean. Geophys. Res. Lett. 35, L15606.
Knee, K.L., Street, J.H., Grossman, E.E., Boehm, A.B., Paytanb, A., 2010. Nutrient inputs to the coastal ocean from submarine groundwater discharge in a groundwater-dominated system: relation to land use (Kona coast, Hawaii, USA). Limnol. Oceanogr. 55, 1105–1122.
Lamborg, C.H., Fitzgerald, W.F., Skoog, A., Visscher, P.T., 2004. The abundance and source of mercury-binding organic ligands in Long Island Sound. Mar. Chem. 90, 151–163.
Laurier, F.J.G., Cossa, D., Beucher, C., Breviere, E., 2007. The impact of groundwater discharges on mercury partitioning, speciation and bioavailability to mussels in a coastal zone. Mar. Chem. 104, 143–155.
Lavoie, R.A., Jardine, T.D., Chumchal, M.M., Kidd, K.A., Campbell, L.M., 2013. Biomagnification of mercury in aquatic food webs: a Worldwide Meta-analysis. Environ. Sci. Technol. 47, 13385–13394.
Lee, Y., Rahman, M.D.M., Kim, G., Han, S., 2011. Mass balance of total mercury and monomethylmercury in coastal embayments of a volcanic island: significance of submarine groundwater discharge. Environ. Sci. Technol. 45, 9891–9900.
Luengen, A.C., Flegal, A.R., 2009. Role of phytoplankton in mercury cycling in the San Francisco Bay estuary. Limnol. Oceanogr. 54, 23–40.
Martinez, J.A., Smith, C.M., Richmond, R.H., 2012. Invasive algal mats degrade coral reef physical habitat quality. Estuar. Coast. Shelf Sci. 99, 42–49.
Mason, R.P., Choi, A.L., Fitzgerald, W.F., Hammerschmidt, C.R., Lamborg, C.H., Soerensen, A.L., Sunderland, E.M., 2012. Mercury biogeochemical cycling in the ocean and policy implications. Environ. Res. 119, 101–117.
Mason, R.P., Lawson, N.M., Lawrence, A.L., Leaner, J.J., Lee, J.G., Sheu, G.R., 1999. Mercury in the Chesapeake Bay. Mar. Chem. 65, 77–96.
Mason, R.P., Reinfelder, J.R., Morel, F.M., 1996. Uptake, toxicity, and trophic transfer of mercury in a coastal diatom. Environ. Sci. Technol. 30, 1835–1845.
Moore, W.S., 2010. The effect of submarine groundwater discharge on the ocean. Annu. Rev. Mar. Sci. 2, 59–88.
Morel, F.M., Kraepiel, A.M., Amyot, M., 1998. The chemical cycle and bioaccumulation of mercury. Annu. Rev. Ecol. Syst., 543–566.
NOAA, 2013. National Weather Service. Honolulu, HI. http://www.prh.noaa.gov/hnl/hydro/pages/rra_graphs.php.
Pacyna, E.G., Pacyna, J., Sundseth, K., Munthe, J., Kindbom, K., Wilson, S., Steenhuisen, F., Maxson, P., 2010. Global emission of mercury to the atmosphere from anthropogenic sources in 2005 and projections to 2020. Atmos. Environ. 44, 2487–2499.
Parker, J.L., Bloom, N.S., 2005. Preservation and storage techniques for low-level aqueous mercury speciation. Sci. Total Environ. 337, 253–263.
Parks, J.M., Johs, A., Podar, M., Bridou, R., Hurt, R.A., Smith, S.D., Tomanicek, S.J., Qian, Y., Brown, S.D., Brandt, C.C., 2013. The genetic basis for bacterial mercury methylation. Sci 339, 1332–1335.
Peterson, R.N., Burnett, W.C., Glenn, C.R., Johnson, A., 2009. Quantification of point-source groundwater discharges to the ocean from the shoreline of the Big Island, Hawaii. Limnol. Oceanogr. 54, 890–904.
Pickhardt, P.C., Fisher, N.S., 2007. Accumulation of inorganic and methylmercury by freshwater phytoplankton in two contrasting water bodies. Environ. Sci. Technol. 41, 125–131.
Presto, M.K., Storlazzi, C.D., Logan, J.B., Reiss, T.E., Rosenberger, K.J., 2012. Coastal Circulation and Potential Coral-larval Dispersal in Maunalua Bay, O'ahu, Hawai'i—Measurements of Waves, Currents, Temperature, and Salinity, June–September 2010, p. 67. U.S. Geological Survey Open-File Report 2012-1040.
Rahman, M., Lee, Y.-g, Kim, G., Lee, K., Han, S., 2013. Significance of submarine groundwater discharge in the coastal fluxes of mercury in Hampyeong Bay, Yellow Sea. Chemosphere 91, 320–327.
Raine, L.M., Siegel, B.Z., McMurtry, G.M., 1995. Mercury accumulation in sediments of the Ala Wai Canal and in soils and stream sediments of the central Honolulu watershed. Pac. Sci. 49, 511–525.
Siegel, S., Siegel, B., 1984. First estimate of annual mercury flux at the Kilauea main vent. Nature 309, 146–147.
Storlazzi, C.D., Presto, M.K., Logan, J.B., Field, M.E., 2010. Coastal Circulation and Sediment Dynamics in Maunalua Bay, Oahu, Hawaii: Measurements of Waves, Currents, Temperature, Salinity, and Turbidity: November 2008—February 2009. U.S. Geological Survey Open-File Report, 2010-1217.
Sunderland, E.M., Krabbenhoft, D.P., Moreau, J.W., Strode, S.A., Landing, W.M., 2009. Mercury sources, distribution, and bioavailability in the North Pacific Ocean: Insights from data and models. Glob. Biogeochem. Cycles 23.
Swarzenski, P., Dulaiova, H., Dailer, M., Glenn, C., Smith, C., Storlazzi, C., 2013. A Geochemical and Geophysical Assessment of Coastal Groundwater Discharge at Select Sites in Maui and O'ahu, Hawai'i, Groundwater in the Coastal Zones of Asia-Pacific. Springer, pp. 27–46.
Swarzenski, P.W., Izbicki, J.A., 2009. Coastal groundwater dynamics off Santa Barbara, California: combining geochemical tracers, electromagnetic seepmeters, and electrical resistivity. Estuar. Coast. Shelf Sci. 83, 77–89.
Swarzenski, P.W., Izbicki, J.A., Grossman, E.E., Glenn, C.R., Plath, C.A., Kelly, J.L., 2009. A multi-proxy approach to submarine groundwater discharge studies: examples from Santa Barbara, CA and Maunalua Bay, HI. In: Geochimica et Cosmochimica Acta, Awards Ceremony Speeches and Abstr.acts of the 19th Annual V.M. Goldschmidt Conference 73, p. A1299.
Swarzenski, P.W., Kindinger, J.L., 2003. Leaky Coastal Margins: Examples of Enhanced Coastal Groundwater/surface Water Exchange from Tampa Bay and Crescent Beach Submarine Spring, Florida, USA. In: Coastal Aquifer Management, Monitoring and Modeling and Case Studies, pp. 93–112.
Swarzenski, P.W., Simonds, F.W., Paulson, A.J., Kruse, S., Reich, C., 2007. Geochemical and geophysical examination of submarine groundwater discharge and associated nutrient loading estimates into Lynch Cove, Hood Canal, WA. Environ. Sci. Technol. 41, 7022–7029.
Szymczycha, B., Miotk, M., Pempkowiak, J., 2013. Submarine groundwater discharge as a source of mercury in the Bay of puck, the southern Baltic sea. Water, Air, Soil. Pollut. 224, 1–14.
Tribble, G.W., 2008. Ground Water on Tropical Pacific Islands: Understanding a Vital Resource. In: US Geological Survey Circular 1312, p. 35.
USEPA, 1997. Mercury Study Report to Congress. In: An Ecological Assessment for Anthropogenic Mercury Emissions in the United States, vol VI. EPA-452/R-97–008, 158.
USEPA, 2002. Method 1631, Revision E: Mercury in Water by Oxidation, Purge and Trap, and Cold Vapor Atomic Fluorescence Spectrometry. EPA-821-R-02–019.
Wolanski, E., Martinez, J.A., Richmond, R.H., 2009. Quantifying the impact of watershed urbanization on a coral reef: Maunalua Bay, Hawaii. Estuar. Coast. Shelf Sci. 84, 259–268.